Computer-assisted stochastic multi-well correlation: Sedimentary facies versus well distality

Paul Baville, Marcus Apel, Silvan Hoth, Dirk Knaust, Christophe Antoine, Cédric Carpentier, Guillaume Caumon

Highlights

Computer-assisted stochastic multi-well correlation: Sedimentary facies *versus* well distality[⋆]

Paul Baville, Marcus Apel, Silvan Hoth, Dirk Knaust, Christophe Antoine, Cédric Carpentier, Guillaume Caumon

- Correlating borehole well data is prone to uncertainty.
- *Principle of correlation*: a facies cannot be correlated to a depositionally shallower (deeper) facies in a more distal (proximal) basin area.
- The proposed method generates consistent chronostratigraphic correlation sets with respect to sedimentary facies and well distality interpretations.
- Distality is key information to produce acceptable correlations.
- We formulated distality as a mathematical rule acting based on facies zonation to inform a dynamic programming correlation algorithm.
- Various consistent correlations are obtained by changing facies definitions and relative distality on a North Sea Jurassic core data.
- Stratigraphic uncertainty directly affects the connectivity of chronostratigraphic units between well data.

Computer-assisted stochastic multi-well correlation: Sedimentary facies *versus* well distality

Paul Baville[a,1], Marcus Apel[b], Silvan Hoth[b], Dirk Knaust[b], Christophe Antoine[a], Cédric Carpentier[a], Guillaume Caumon[a]

[a] *Université de Lorraine, CNRS, GeoRessources, 54000 Nancy, France*
[b] *Equinor ASA, 4035 Stavanger Norway*

Abstract

To reflect interpretation uncertainties, an increasing number of interpreters may generate different sets of correlations from the same data set. To reduce human interpretation bias, we use a computer-assisted method for generating stochastic multi-well correlations to be used in uncertainty studies. This method relies on a translation of sedimentary concepts into cost functions that are related to each possible correlation. All these correlation costs are used to populate a cost matrix in order to apply the Dynamic Time Warping algorithm and to compute the n-best correlation sets having the n-least cumulative costs. The proposed cost function reflects prior knowledge about sediment transport direction, and it is tested on two wells from the North Sea, which penetrate a Middle Jurassic reservoir interval. Well markers are described by two parameters: (1) the sedimentary facies representing the depositional environment, and (2) the relative distality of the well computed from its position along the sediment transport direction. The main *principle of correlation* used in this article follows Walther's Law of Facies: a well marker (described by facies and distality) cannot be correlated with another well marker described by a depositionally deeper facies at a more proximal position, or a depositionally shallower facies at a more distal position. This approach produces consistent stratigraphic correlations, and highlights the sensitivity of the solution to the facies zonation and to the relative disability. Therefore, the proposed rule offers a way to coherently consider chronostratigraphic correlation and the associated uncertainties at a scale smaller than generally considered in deterministic correlation.

Keywords: Stratigraphy, Well Correlations, Sedimentary Facies, Well Distality, Walther's Law of Facies, Dynamic Time Warping.

⋆Author's postprint version. Published in Marine and Petroleum Geology 135 (Jan 2022), 105371 .doi:10.1016/j.marpetgeo.2021.105371

Email address: paul.baville@univ-lorraine.fr (Paul Baville)

Introduction

The stratigraphic correlation of sedimentary rock series observed in borehole data or outcrops is a common procedure in basin studies. Correlation affects the understanding of sedimentary deposits, the quantitative analysis of subsurface resources and source-to-sink models. In order to predict the subsurface geometry, stratigraphy is used to correlate sedimentary horizons from sparse wells (e.g., Nagy and Bjørlykke, 2015). These correlations may be done at a large scale from reflection seismic data, or at a smaller scale from well data. In both cases, the main objective of the stratigraphic correlation is to determine the surfaces bounding the stratigraphic units, where geometry can then be predicted away from observations.

In this work, we focus on stratigraphic correlation generated from well data (small vertical meter-scale and large horizontal kilometer-scale). There are two types of well data: (1) well logs, corresponding to quasi-continuous (regular sampling) geophysical measurements along the well path (e.g., gamma ray, sonic, neutron porosity), and (2) well zones, corresponding to categorical reservoir properties and defined by their top and bottom depths along the well path (e.g., biozones, coarsening-up intervals, structural zones, sedimentary facies).

Well correlation may be achieved manually by experts using well log and core sample interpretations (e.g., Bourquin et al., 1998). The resulting scenario is a correlation set. This process generally involves iteration between the identification of intervals or markers on each well, and the correlation of these features across wells. Although uncertainties in correlation exist, a geologist generally proposes the "best case" scenario based on a careful data analysis and in accordance to their experience, or sometimes more (two to five) scenarios, reflecting some - but not all - interpretation uncertainties. Increasing the number of interpreters may help to gain confidence about a particular interpretation, or conversely to produce more scenarios.

Ideally, a quantification of correlation uncertainties would call for generating every possible scenario and to evaluate their likelihood. However, the very large number of possible scenarios makes their manual validation almost impossible. To overcome this limitation, a numerical method to provide automatically multiple stratigraphic scenarios is proposed (e.g., Pels et al., 1996; Lallier et al., 2016; Edwards et al., 2018). The scenarios are consistent with the input data and with some explicitly defined stratigraphic concepts, which guarantee that the solutions are acceptable.

In this paper, we consider chronostratigraphic principles (Section 1), which are considered as the most predictive to model the subsurface. Among chronostratigraphic approaches, sequence stratigraphy describes the stratigraphic structure of sedimentary basins based on depositional sequences (e.g., Mitchum et al., 1977; Galloway, 1989; Catuneanu et al., 2011). Depending on the well distality

(well position along a proximal-to-distal transect), depositional processes vary and lead to different isochronous sedimentary facies and vertical stacking patterns (e.g., Borgomano et al., 2008; Bhattacharya, 2011; Lallier et al., 2016; Knaust and Hoth, 2020).

To retrieve such isochronous surfaces from stratigraphic series, we rely on the Dynamic Time Warping algorithm (Section 2). This numerical tool computes the likelihood of a correlation set among all possible correlation sets and returns the best correlation set, i.e., the most likely correlation set (Sakoe and Chiba, 1978; Waterman and Raymond, 1987; Hale, 2013; Wheeler and Hale, 2014) or the n-best correlation sets (Pels et al., 1996; Lallier et al., 2016; Edwards et al., 2018). The likelihood of one correlation set is computed by minimizing the cumulative cost of correlations and transition between correlations. In this paper, the key methodological contribution is the explicit integration of distality in the elementary correlation costs of the Dynamic Time Warping. This enables to compute global correlation likelihood and to rule out impossible lateral facies variations along the generated isochronous layers.

In this method, all input data (well logs and core samples of the interval of interest) must be acquired within unfaulted stratigraphic parasequence successions. This consideration may be justified in the presence of seismic data or dipmeter data analysis. We focus on relative chronostratigraphic well marker correlation based on (1) the sedimentary facies, that represents the depositional environment interpreted as zones along the well paths, and (2) the relative distality of the well along the sediment transport direction. The proposed method is first validated with a simple synthetic data set (Section 2.3) and secondly applied on an unfaulted (validated by dipmeter data) sedimentary coastal deltaic data set from the South Viking Graben in the North Sea (Knaust and Hoth, 2020) (Section 3).

1. Conceptual stratigraphic correlation framework

1.1. Lithostratigraphy versus chronostratigraphy

Considering the empirical *principle of superposition* stating that "*strata have been deposited above older strata than themselves*" (Steno, 1669), stratigraphy can be interpreted in, at least, two different ways (Figure 1) and may lead to very distinct correlations with direct implication for paleogeography and reservoir connectivity:

- *Lithostratigraphy* correlates strata by comparing their composition or rock type. Well markers are correlated if they are similar (or, even better, identical) (Figure 1.A) to generate layers or beds containing the same facies (*characteristics*) (Figure 1.B). However, this method does not consider possible lateral shifts of facies along a proximal-to-distal direction in the basin.

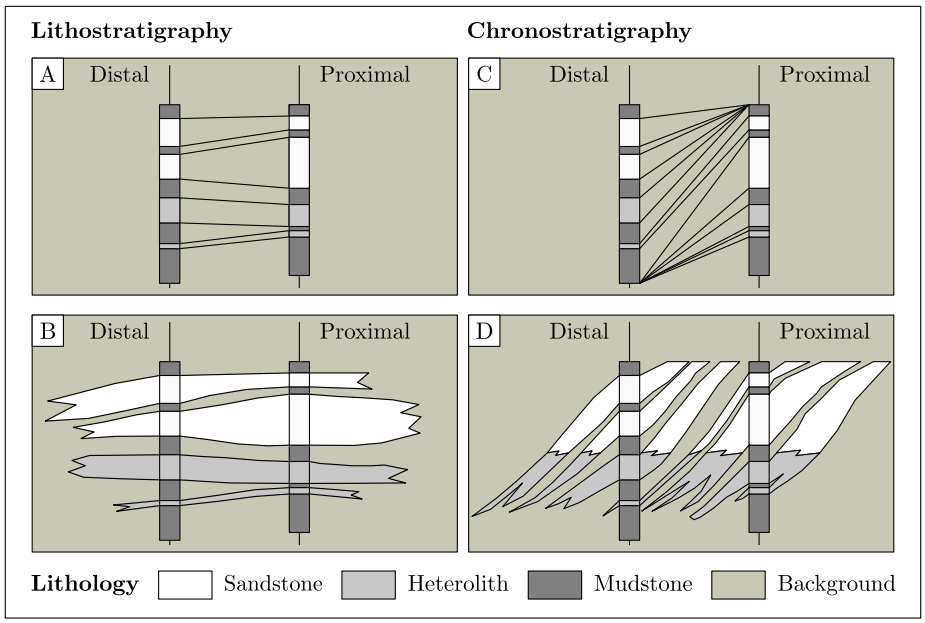

Figure 1: Lithostratigraphic (left) and Chronostratigraphic (right) facies correlation and geological layers interpolation from the same data set. Inspired by Ainsworth et al. (1999). (single column - colored)

- *Chronostratigraphy* correlates strata by comparing their geological age and therefore correlates well markers when they are deemed to correspond to the same depositional time-window (Figure 1.C). This generates layers bounded by isochronous horizons, which may have lateral facies variations depending on depositional environments tending to produce realistic facies connectivity (Figure 1.D). Chronostratigraphic correlations consider lateral shifts of facies to be possible along time lines. Consequently stratal geometry and connectivity patterns illustrated in Figure 1 are very different depending on the correlation method used.

Sedimentary reservoir correlation is usually based on deterministic well-data analysis. Correlating these data is essential in subsurface modeling prior to defining the geometry of geobodies and to model their petrophysical properties. In quantitative subsurface modeling and sedimentological studies, chronostratigraphic time line interpretation is generally preferred to lithostratigraphic principles because it best reproduces the lateral and vertical facies variations derived from depositional processes and the continuity of thin beds (Figure 1) (e.g., Ainsworth et al., 1999). However, lithostratigraphy is often used to complement chronostratigraphy when observations are closer than the lateral size of sedimentary bodies and the chronostratigraphic resolution.

1.2. Sequence stratigraphy

Sequence stratigraphy provides several concepts and methods to analyze, characterize and predict stratigraphic and sedimentary architecture in the subsurface. The main idea is to subdivide the sedimentary strata into several stratigraphic sequences based on genetic considerations about the depositional history (Sloss et al., 1949). A sequence is defined as "a relatively conformable succession of genetically related strata bounded by unconformities or their correlative conformities" (Mitchum, 1977). The key idea of sequence stratigraphy is to relate stratigraphic units to cycles of accommodation and sedimentation rate, which are controlled by global (eustatic) seal-level changes, local paleotopography, subsidence, and climate (Johnson and Murphy, 1984; Galloway, 1989; Ruiz and Le Nir, 1999; Catuneanu et al., 2011). This concept leads to several depositional system tracts subdividing these sequences (Catuneanu, 2002):

- The *Transgressive system tract* develops during a period of positive accommodation a, which is not compensated by sedimentation rate s ($a/s > 1$). The vertical stacking of facies is fining-upward for both marine and alluvial environments, coeval with a backstepping of coastal marine facies in a landward direction. The system tract is bounded at the top by a maximum flooding surface.

- The *Regressive system tract* includes all regressive deposits corresponding to two successive system tracts:

    1. The *Highstand system tract* is formed when the sedimentation rate becomes larger than the accommodation (normal regression, $0 < a/s < 1$) (Catuneanu et al., 2009). A part of the sediment volume is stacked vertically (aggradation), but the excess material is deposited ahead of the depositional system (progradation). This system tract starts just above the maximum flooding surface and includes, in marine settings, coarsening-upward (prograding) deposits.
    2. The *Lowstand system tract* is formed after a period of negative accommodation (forced regression, $a < 0$) at the beginning of a renewal in accommodation, when the sedimentation rate is larger than the rate of accomodation (normal regression, $0 < a/s < 1$). Its upper limit is the maximum regressive surface, which can merge with the transgression surface (Embry, 2009). In marine settings, it is characterized by coarsening-upward deposits, which are not necessarily entirely preserved due to ravinement erosion during transgression.

These different system tracts correspond to successions of regressive and transgressive periods recorded in sediments (Figure 2.A).

Wheeler (1958) proposed combined diagrams, which show the same stratigraphic section using two different representations: (1) a stratigraphic section as function of depth, and (2) a stratigraphic section as function of geological age (Figure 2.B) (Driscoll and Karner, 1999; Mallet, 2004; Holbrook and Bhattacharya,

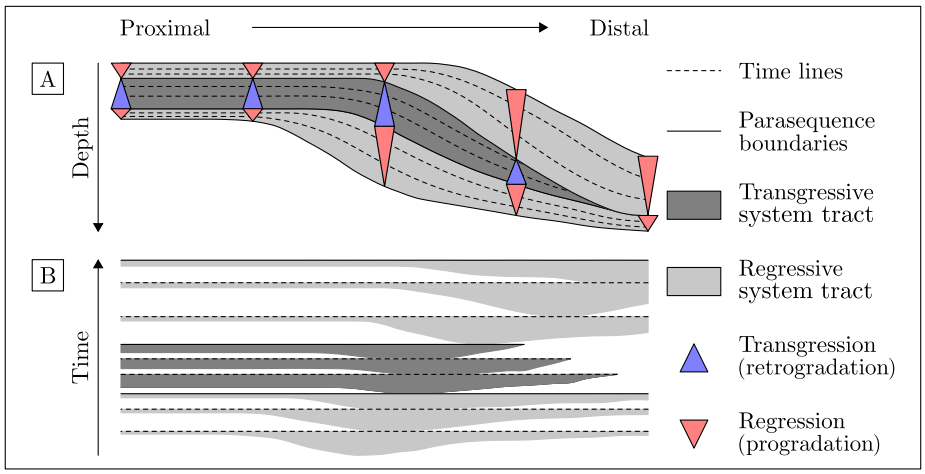

Figure 2: Successive transgressive and regressive parasequences corresponding respectively to transgressive and regressive system tracts. Inspired by Kedzierski et al. (2008). (A) Depth cross-section and (B) time cross-section (Wheeler diagram; Wheeler (1958)). (single column - colored)

2012; Amosu and Sun, 2017; Qayyum et al., 2017).

Sedimentary facies description helps in the interpretation of the paleoenvironment and depositional event successions along the well path. While the herein proposed method is in general applicable to various sedimentary environments, it has been applied to marginal-marine deltaic wave-dominated deposits.

1.3. Principle of correlation

In this work, relative chronostratigraphy is used to associate well markers. The objective of this work is to correlate time windows. We can assume that over a given area, some deposition events are quasi-synchronous depending on basin geometry, subsidence, distribution and depositional system. Therefore, along a given isochronous surface, all deposits have (approximately) the same geological age (Figure 2.B). In this case, correlating these isochronous deposits is the same as correlating time windows and *vice versa*.

A sedimentary domain can be characterized by two main directions: proximal-to-distal direction (dip), given by the regional sediment transport direction, and the direction perpendicular to it (depositional strike). In practice, these two directions may change laterally (e.g., in fan-shaped deltas), but, for simplicity the case of a Cartesian geometry is considered here to schematize the internal structure of a sedimentary basin margin (Figure 3). In the direction of sediment transport (BB'), there is a superposition of sigmoidal bodies whereas along the depositional strike direction (AA'), a superposition of monoclinal bodies occurs.

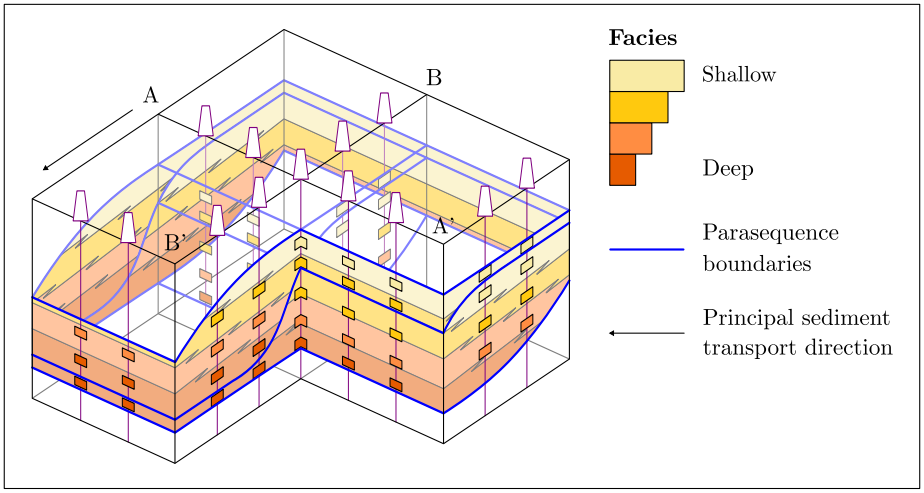

Figure 3: Three-dimensional illustration of a simplified sedimentary basin margin geometry along the depositional strike direction (AA') and the principal sediment transport direction (BB'). Parasequence boundaries (blue lines) are isochronous lines separating clinoforms. (single column - colored)

These sedimentary bodies are defined as clinoforms (Rich, 1951) and are sets of facies (from the most proximal to the most distal region) during the same depositional event. Depending on the context (distance to fluvial sediment source, dominance of waves / tides in the depositional process), clinoforms are observed in every direction, even though they have different shapes along depositional strike or sediment transport direction.

Figure 3 illustrates two successive clinoforms formed during a normal regression and bounded by isochronous surfaces (blue lines). These two clinoforms may be divided into four sedimentary facies classified by their relative depositional depth. These clinoforms may be defined at a large time interval (4th order - parasequences), in the range of 150 000 to 200 000 years (Knaust and Hoth, 2020). And at a lower scale, clinoforms can be subdivided in several stratigraphic system tracts.

A clinoform may be subdivided into several sequences and the purpose of this work is to correlate well markers in order to reproduce these subdivisions and to generate a chronostratigraphic model of the subsurface.

Figure 4 illustrates that along the two principal directions, well marker correlation likelihood may be qualitatively evaluated by applying Walther's Law of Facies. This leads to several configurations, which are not plausible if we assume that the depositional depth increases with distality:

- A sedimentary facies in a well cannot be associated with a depositionally

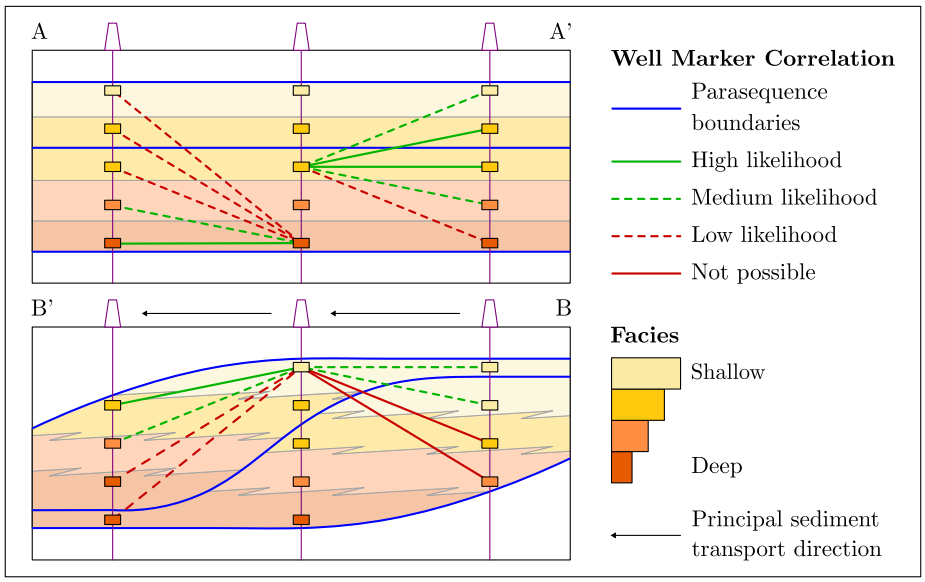

Figure 4: Well marker correlation likelihood based on facies association within a sedimentary basin along the depositional strike direction (AA') and the principal sediment transport direction (BB'). Parasequence boundaries (blue lines) are isochronous lines separating clinoforms. Facies associations are represented by dashed or full green or red lines according to their likelihood. (single column - colored)

shallower facies in a more distal well.

- A sedimentary facies in a well cannot be associated with a depositionally deeper facies in a more proximal well.

Considering these two conditions, it is possible to postulate a *principle of correlation* stating that *a well marker (described by facies and distality taken at the center of an interval having a constant facies and a constant distality) cannot be correlated with another well marker described by a depositionally deeper facies at a more proximal position, or a depositionally shallower facies at a more distal position.*

This principle allows us to evaluate every single well marker correlation line independently and not the entire correlation set. Therefore, the next section focuses on the computation of likely correlation sets.

2. Correlation likelihood computation - Dynamic Time Warping

The Dynamic Time Warping algorithm is a dynamic programming method which can be used to quantify the likelihood of a large number of scenarios by finding the best one (Sakoe and Chiba, 1978). In our method, we use the two-dimensional Dynamic Time Warping algorithm, implying that we compare

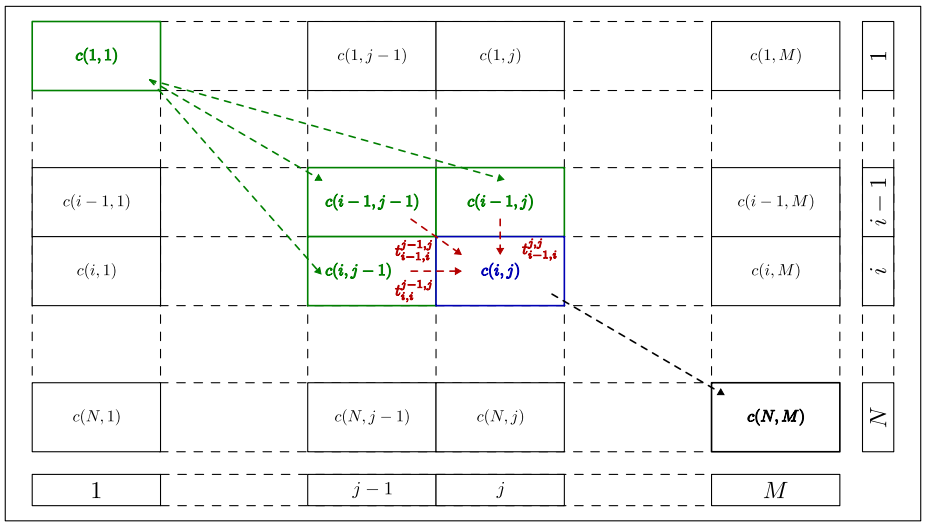

Figure 5: Illustration of the Dynamic Time Warping algorithm at step (i, j) with two wells containing N and M markers. (single column - colored)

two wells composed of N markers and M well markers respectively. Each pair of markers (i, j) has a correlation cost $c(i, j)$, and each transition between two correlations (i, j) and (k, l) has a transition cost $t_{i,k}^{j,l}$ as illustrated in Figure 5.

Correlation and transition costs are computed for every possible well marker correlation and correlation transitions. Assuming that extremities of the two wells are correlated, for each scenario, the global cost is computed iteratively from the top correlation $(1, 1)$ to the bottom correlation (N, M) given by: $\forall\ (i, j) \in [\![1, N]\!] \times [\![1, M]\!]$,

$$C(i,j) = c(i,j) + min \begin{pmatrix} t_{i-1,i}^{j,j} & + & C(i-1,j) \\ t_{i-1,i}^{j-1,j} & + & C(i-1,j-1) \\ t_{i,i}^{j-1,j} & + & C(i,j-1) \end{pmatrix}. \quad (1)$$

Figure 5 illustrates the two-dimensional Dynamic Time Warping algorithm. Considering two wells composed of N markers and M markers respectively, it is possible to generate a two-dimensional matrix where each cell $c(i, j)$ corresponds to the correlation (i, j). Each cell is filled by the correlation cost $c(i, j)$ and is linked to its three up-and-left neighbors by the transition cost $t_{i-1,i}^{j-1,j}$ (red-arrows). The Dynamic Time Warping algorithm iteratively minimizes the global cost and keeps the previous path with the lowest cost $C(i - 1, j - 1)$ (green-arrows). The algorithm ends when it reaches the last correlation (N, M) (black-arrow).

Dynamic Time Warping was initially introduced in stratigraphic applications to correlate facies (Smith and Waterman, 1980; Waterman and Raymond, 1987)

and can also be used to correlate well-logs (Hale, 2013; Wheeler and Hale, 2014; Wu et al., 2018). For relative chronostratigraphy, the main difficulty is to define appropriate correlation costs c and transitions costs t. For example, Lallier et al. (2016) used paleobathymetry and depositional slope constraints to define carbonate facies correlation rules. Edwards et al. (2018) derived correlation and transition costs by scanning three-dimensional models obtained by process-based stratigraphic simulation. These approaches can incorporate depositional concepts into automatic correlation, but they call for determining quantitative parameters which may be difficult to infer in some depositional environments. In the next subsection, we use the more qualitative notion of distality discussed in Section 1.3 to define new correlation costs $c(i, j)$.

2.1. Correlation cost computation - $c(i, j)$

If we consider Figure 3 as a simple approximation for a sedimentary basin margin geometry along the depositional strike direction (AA') and depositional dip direction (BB'), it is possible to qualitatively estimate the well marker correlation likelihood as illustrated in Figure 4.

Input data are (1) sedimentary facies interpretation defined along the entire well by their top and bottom depths, and (2) well distality defined by a piecewise constant function of the depth according to the depositional context. The proposed method may be applied on two wells, referred to as well 1 and well 2. For each well, well markers are taken at the center of each sedimentary facies, and assigned to f directly given by the sedimentary facies encoding (facies codes increase from the deepest ($f = 1$) to the shallowest sedimentary facies). Well distality d may vary along a vertical well, but is assumed to be constant within a clinoform (distality is increasingly defined from the most distal position within the basin ($d = 1$) to the most proximal position within the basin), i.e., a parasequence. Note that this ordering can be reversed as long as facies depositional depth and distality are encoded consistently.

Considering that well 1 is composed of N markers $m_1(i)$, $i \in [\![1, N]\!]$ and well 2 is composed of M markers $m_2(j)$, $j \in [\![1, M]\!]$, each marker $m_1(i)$ and $m_2(j)$ can be expressed as:

$$m_1(i) = \{f_1(i), d_1(i)\} \ , \ m_2(j) = \{f_2(j), d_2(j)\}. \tag{2}$$

In order to make every correlation (i, j) comparable, their generation are based on adimensional terms $f(i, j)$ and $d(i, j)$ computed from normalization terms f_0 and d_0 computing respectively from the maximum facies and distality variations observed between the two wells:

$$f_0 = \underset{i,j}{max}(|f_1(i) - f_2(j)|) \ , \ d_0 = \underset{i,j}{max}(|d_1(i) - d_2(j)|). \tag{3}$$

The terms $f(i, j)$ and $d(i, j)$ are given by

$$f(i,j) = \frac{|f_1(i) - f_2(j)|}{f_0} \ , \ d(i,j) = \alpha \times \frac{|d_1(i) - d_2(j)|}{d_0}, \tag{4}$$

where α is a scaling coefficient representing how the lateral size of the depositional is deemed to scale with the inter-well distance.

Based on a conceptual sedimentary basin geometry illustrated in Figure 3 and on the *principle of correlation* considering that a facies cannot be associated with a depositionally shallower (respectively, deeper) facies in a more distal (respectively, proximal) well, it is finally possible to define two possible cases:

1. Facies and distality interpretations are inconsistent with the *principle of correlation*, this way the correlation cost is given by

$$c(i,j) = +\infty. \tag{5}$$

2. Facies and distality interpretations are consistent with the *principle of correlation*, then the correlation cost is given by (Figure 6)

$$c(i,j) = (d(i,j) - f(i,j))^2. \tag{6}$$

This cost function may be analyzed for several cases:

- $d(i,j) = 0$ (wells are orthogonal to the transport direction). In this case, facies are preferentially associated if their depositional depths are similar and the cost function is assimilated to the normalized facies variance given by:

$$c(i,j) = f(i,j)^2 = \left(\frac{|f_1(i) - f_2(j)|}{f_0}\right)^2. \tag{7}$$

- $d(i,j) = 1$ (wells are parallel to the transport direction and have extreme distality values). In this case, facies are preferentially associated if their depositional depths are different, and the cost function is assimilated to the opposite of the normalized facies variance:

$$c(i,j) = (1 - f(i,j))^2 = \left(1 - \frac{|f_1(i) - f_2(j)|}{f_0}\right)^2. \tag{8}$$

- In all the other cases, the cost function (6) entails that the closer the distality, the higher the correlation likelihood between facies having similar depositional depths (Figure 6).

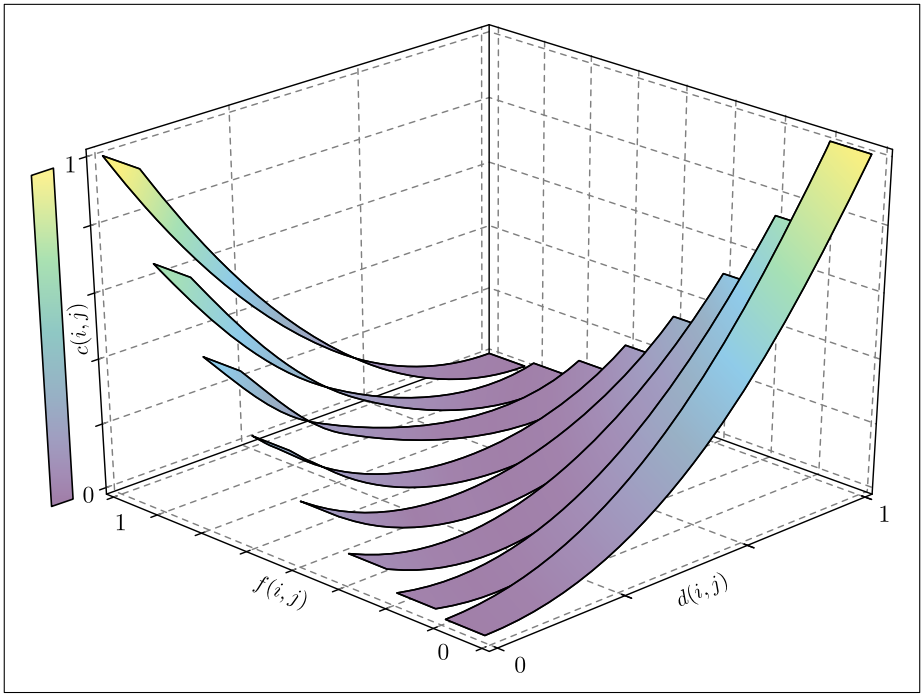

Figure 6: Cost function computing the correlation cost between two well markers based on relative sedimentary facies and relative well distality variations. $f(i,j)$ and $d(i,j)$ are normalized parameters given by Equation (4) and $c(i,j)$ is given by Equation (6). (single column - colored)

2.2. Transition cost computation - $t_{i,k}^{j,l}$

According to the cost matrix illustrated in Figure 5, each well marker correlation is preceded by one well marker correlation among three possible correlations (red arrows) and their transitions are more or less likely. Transition costs are included within the Dynamic Time Warping algorithm to constrain the result as expressed in Equation (1).

Currently, our method does not compute transition costs from input data. These vertical and horizontal transitions within the cost matrix correspond to gaps in correlation sets. In Dynamic Time Warping, gaps are naturally penalized as the diagonal path in the cost matrix minimizes the number of transitions. However, to further penalize stratigraphic gaps, we decide to define a non-zero constant gap cost given by $t_{i,i}^{j-1,j} = t_{i-1,i}^{j,j} = 0.1$ and $t_{i-1,i}^{j-1,j} = 0$.

In this case, $0 \leq c(i,j) + t_{i-1,i}^{j-1,j} \leq 1.1$, and the current cost is no more normalized. A new correlation cost $c^*(i,j)$ is therefore given by $c^*(i,j) = 0.9 \times c(i,j)$, so that $0 \leq c^*(i,j) + t_{i-1,i}^{j-1,j} \leq 1$ is attributed to admissible correlations.

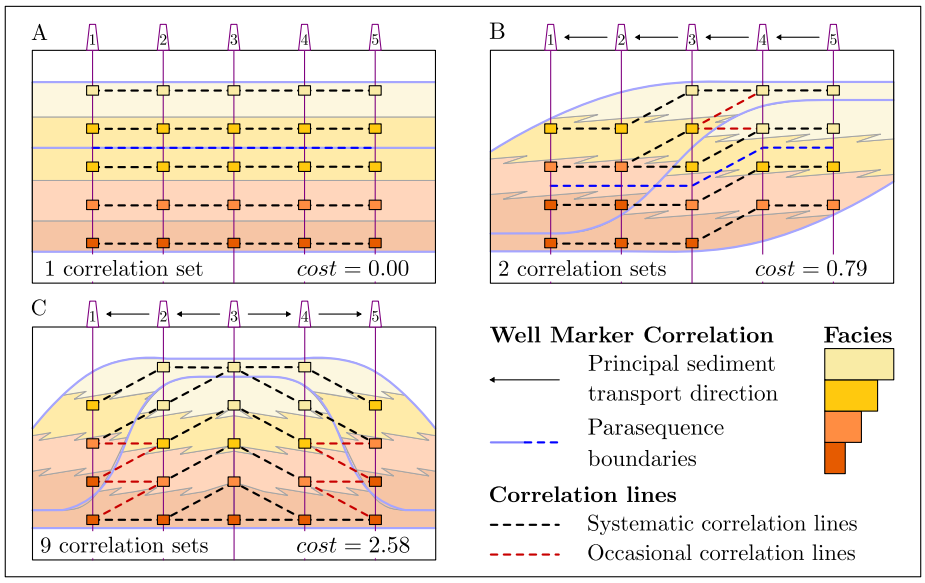

Figure 7: Application of the proposed cost function on three synthetic data sets. (A) Sedimentary basin margin transversal cross-section. (B) Sedimentary basin margin or deltaic longitudinal cross-section. (C) Sedimentary deltaic transversal cross-section. For each scenario, we consider only scenarios having the lowest cumulative cost represented by dashed lines. Black lines are correlations occurring in all realizations, and red lines are correlations which are not systematic. (single column - colored)

2.3. Synthetic data set

The proposed correlation cost function is first tested on synthetic data illustrated in Figure 7. Each scenario is composed of five wells (1,2,3,4,5), so we apply the Dynamic Time Warping method incrementally by defining a correlation path and computing the costs between each added well and the closest well already processed (Lallier et al., 2016).

In our examples, wells are ordered and correlation sets are computed between two successive wells, that is (1-2), then (2-3), then (3-4) and then (4-5). We generated the most likely solutions for each synthetic data set.

This synthetic data set is composed of three simple scenarios based on simple sedimentary basin geometries:

A. Sedimentary basin margin transversal cross-section. All the considered wells have the same distality, so the correlation cost $c(i, j)$ is computed using Equation (7). The best correlation set having the lowest cumulative cost $C = 0.00$ is unique and corresponds to a layer cake correlation (Figure 7.A). The outcome is consistent because all facies are similar along correlation lines. Hypothetical parasequence boundaries may be interpreted as horizontal lines.

B. Sedimentary basin margin or deltaic longitudinal cross-section. The distality increases along the distal-to-proximal transect ($1 \leq d_n(i) \leq 5$) and the correlation cost $c(i, j)$ is computed using Equation (6). There are two correlation sets which reach the lowest cumulative cost $C = 0.79$ (Figure 7.B). Black dashed lines are correlation lines which occur in the two scenarios, and red dashed lines show differences between the two equivalent realizations. Outcomes are consistent because along the sediment transport direction, depositionally deep facies in distal wells are correlated with depositionally shallow facies in proximal wells. These two realizations return three separated correlation groups (connected correlation lines), and hypothetical parasequence boundaries may be interpreted as lines separating two successive chronostratigraphic layers.

C. Sedimentary deltaic transversal cross-section. The distality increases from the center ($1 \leq d_n(i) \leq 3$) and the correlation cost $c(i, j)$ is computed using the distality costs (5) and (6). There are nine correlation sets which reach the lowest cumulative cost $C = 2.58$. Figure 7.C illustrates these realizations in black and red dashed lines. Outcomes are more difficult to evaluate than in scenarios A and B, but they are relatively close to the simplified subsurface model shown in the background.

The reference correlation set is recovered, but it has the same cost as some correlation sets which cross the reference time lines. This illustrates the indeterminacy of the interpretation based solely on incomplete data and on the proposed cost. In cases B and C, it is important to note that the number of realizations costing the less is smaller than expected because of the sequential nature of the correlation. Alternative correlations could be obtained by randomizing the correlation order.

3. Application: Hugin Formation, Gudrun-Sigrun Field, North Sea

The proposed method for computing the likelihood of a well marker correlation from sedimentary facies and well distality yields promising results on simple synthetic data sets and is now applied to a real data set from the North Sea. This data set consists of several wells drilled in the South Viking Graben targeting a Middle Jurassic sandstone reservoir. The interval of interest is the Hugin Formation (Early Callovian part) within the Gudrun-Sigrun Field area (North Sea Block 15/3) (Knaust and Hoth, 2020).

3.1. Stratigraphy and sedimentary context

Based on dipmeter data analysis and biostratigraphic interpretation, the Hugin Formation within the Gudrun-Sigrun Field area appears as an unfaulted chronostratigraphic unit. Its top and bottom are highlighted in seismic images by coal bed reflectors. However, the three-dimensional geometry of the Hugin Formation cannot be interpreted from seismic data and can only be determined from

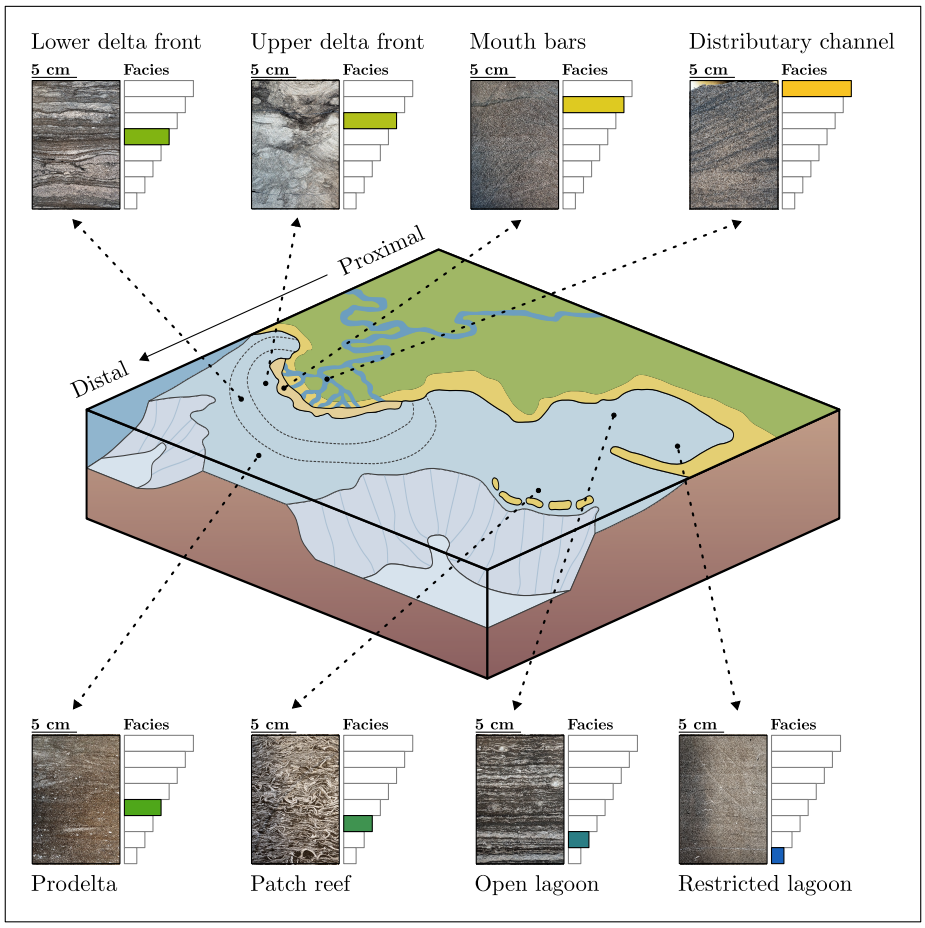

Figure 8: Depositional environment of different sedimentary facies interpreted by Knaust and Hoth (2020) from core samples of the Hugin Formation (Bathonian-Callovian) in two wells in the South Viking Graben, North Sea. (single column - colored)

well data (Knaust and Hoth, 2020).

From drilled and partially cored wells in the zone of interest, well logs and core samples were analyzed to define eight sedimentary facies (Figure 8) and described by Knaust and Hoth (2020) as the bottom "*part of idealized shallowing-upward successions that are bounded by marine flooding surfaces interpreted and therefore are interpreted as parasequences* [...] *and prograding delta lobes*":

1. Restricted lagoon. "*Dark-grey mudstone with planar or low-angle lamination marks the first lithofacies type above the marine flooding surfaces.* [...] *Laminated mudstone represents the deepest and most distal lithofacies* [...] *deposited in a restricted coastal lagoon*" (Knaust and Hoth,

2020).

2. Open lagoon. "*A dark-grey mudstone gradually develops from the underlying laminated mudstone and intergrades with oyster shell beds.* [...] *Sandy to bioclastic mudstone is genetically related to the laminated mudstone but increased sandy input and scattered oyster bioclasts indicate a more open lagoon nearby local oyster patch reefs or biostromes (comparable to the forereef facies) in the distal vicinity of a bay-head prodelta*" (Knaust and Hoth, 2020).

3. Patch reef. "*This lithofacies type occurs above the sandy to bioclastic mudstone, more rarely above the laminated mudstone, or interbedded with the mudstone facies with either gradual or sharp boundaries.* [...] *The oyster shell beds are a common lithofacies type in the Gudrun-Sigrun area and represent oyster patch reefs on local highs within the low-energy open lagoon with a brackish environment (Koppka, 2015)*" (Knaust and Hoth, 2020).

4. Prodelta. "*Brownish-grey, heterogeneous siltstone with admixtures of mud and sand is typically intercalated between mud-rich lithofacies types below and sand-dominated lithofacies above.* [...] *Based on its position within the shallowing-upward succession, the heterogeneous siltstone facies is interpreted as prodelta facies belt in front of a bay-head delta (e.g. Bhattacharya, 2006)*" (Knaust and Hoth, 2020).

5. Lower delta front. "*Brownish-grey sandstone and siltstone layers are intercalated with dark-brown mudstone drapes, thinly bedded but slightly thickening-upwards beds.* [...] *Heterolithic sandstone originated in a distal part of a prograding bay-head delta in the lower delta front (e.g. Bhattacharya, 2006)*" (Knaust and Hoth, 2020).

6. Upper delta front. "*This lithofacies type consists of light-grey, silty to muddy, fine-grained sandstone beds with a thickening and coarsening-upward trend.* [...] *Bioturbated sandstone is a part of the upper delta front of a bay-head delta*" (Knaust and Hoth, 2020).

7. Mouth bar. "*Thickly bedded, brownish-grey, fine-to medium-grained and moderately to well sorted sandstone occurs in close association with bioturbated and heterolithic sandstone.* [...] *The facies association, grain size, sorting, sedimentary structures and bioturbation of this sandstone support an interpretation as mouth-bar deposits occurring at the termination of distributary channels and within the upper delta-front area (e.g. Jerrett et al., 2016)*" (Knaust and Hoth, 2020).

8. Distributary channel. "*Brownish-grey, medium- to coarse-grained sandstone occurs in thick beds with basal and internal erosion surfaces.* [...] *The stratigraphic context suggests deposition in distributary channels*" (Knaust and Hoth, 2020).

These facies codes are globally ordered by decreasing distality from 1 to 8, so they can be used directly in Equation (6). Moreover, facies can also be grouped before correlation to reduce complexity, and assess the impact of the level of interpretation detail on the correlation outcomes. To this end, the eight initial facies are grouped in three possible facies associations according to their depositional positions along a distal-to-proximal transect:

A. Sedimentary facies are divided into three groups. (1) Distal sedimentary facies 1-3 corresponding to depositional environments from restricted lagoons to patch reefs. (2) Intermediate sedimentary facies 4-6 corresponding to deltaic environments from the prodelta to the upper delta front. (3) Proximal sedimentary facies 7-8 corresponding to mouth bars and distributary channels.

B. Sedimentary facies are divided into three groups. (1) Distal sedimentary facies 1-3 corresponding to depositional environments from restricted lagoons to patch reefs. (2) Intermediate sedimentary facies 4 corresponding the prodelta. (3) Proximal sedimentary facies 5-8 corresponding to depositional environments from the lower delta front to distributary channels.

C. Sedimentary facies are divided into two groups. (1) Distal sedimentary facies 1-4 corresponding to depositional environments from restricted lagoons to the prodelta. (2) Intermediate sedimentary facies 5-8 corresponding to depositional environments from the lower delta front to distributary channels.

3.2. Well data

The proposed correlation cost function based on sedimentary facies and well distality is applied on two wells, well 1 and well 2 from the Gudrun-Sigrun Field area. These two wells are fully cored in the bottom part of the Hugin Formation and biostratigraphic analysis performed. It confirms that the lower part of the Hugin Formation in wells 1 and 2 have the same geological age (i.e., Early Callovian) (Figure 9).

During the Early Callovian, deposits in wells 1 and 2 were part of the same bayhead delta sourced with sediments from East to Northeast (Knaust and Hoth, 2020). Based on the depositional environment classification, sedimentary facies are interpreted along the lower part of the Hugin Formation in well 1, referred to as the distal well because of its western position, and in well 2, referred to as the proximal well because of its eastern position (Figure 9). It is assumed that distality is constant in each well ($d_1(i) = 1$ and $d_2(j) = 2$ in Equation (4)). This assumption is based on a stable direction of sediment transport during the considered time interval, which is supported by dipmeter data.

Additionally, transgressive and regressive parasequences (T-R parasequences) were interpreted along these two wells. This correspondence is supported by

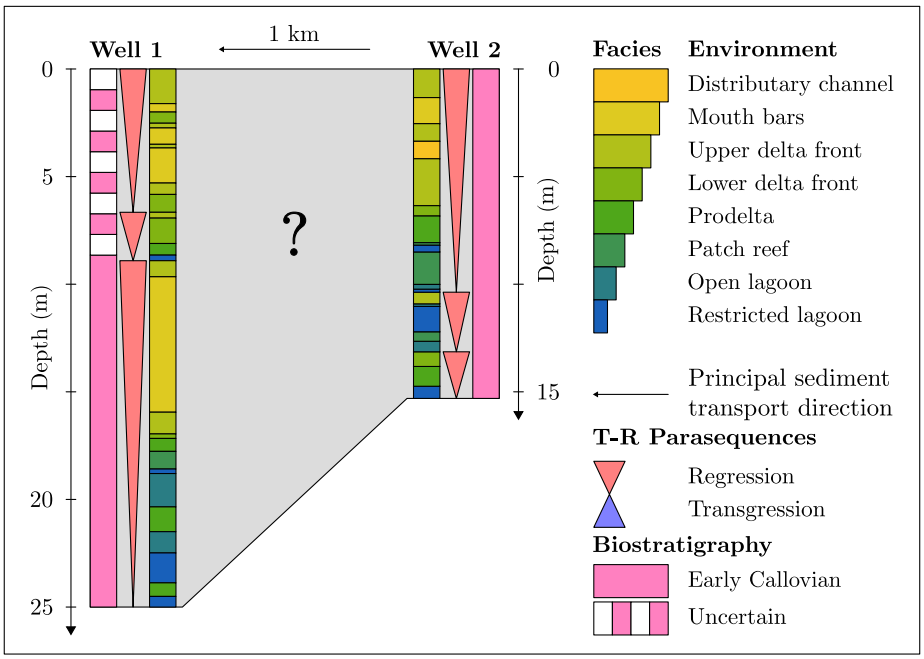

Figure 9: Sedimentary facies, parasequence and biostratigraphic interpretation along wells 1 and 2 in the lower part of the Hugin Formation within the Gudrun-Sigrun Field area (Knaust and Hoth, 2020). (single column - colored)

biostratigraphic interpretation and by the identification of major marine flooding events characterized by reworked sediments and scattered peebles above these ravinement surfaces (Knaust and Hoth, 2020). However, it is important to note that no absolute evidence exists about how these regressive sequences are correlated between both wells. The deepest parasequence identified in well 1 and the shallowest parasequence identified in well 2 (Figure 9) are analyzed by Knaust and Hoth (2020) and dipmeter data acquired in these parasequences confirm a sediment transport direction towards West-Southwest, i.e., from well 2 to well 1.

4. Results and interpretations

Simulating computer-assisted correlations on this data set involves computing a correlation cost $c(i, j)$ for each possible well marker correlation. First, a correlation cost minimizing the facies variance is computed from the interpreted well markers using Equation (7), corresponding to lithostratigraphic correlation. Then, the distality correlation cost function is applied on the data using Equation (8), and on the three different facies associations defined in Section 2.3.

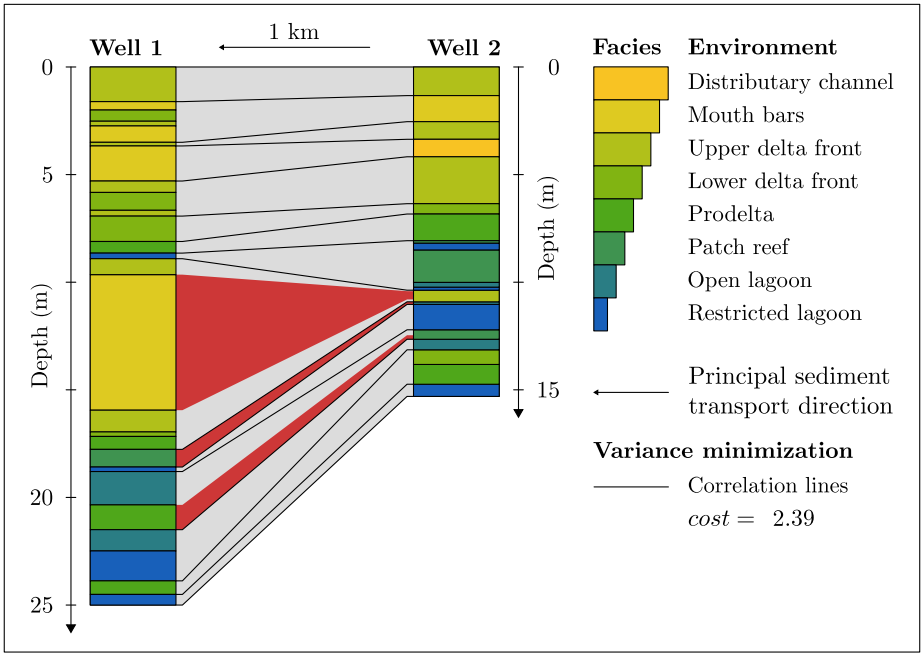

Figure 10: The correlation set having the lowest cumulative correlation cost computed using Equation (7), corresponding to a lithostratigraphic concept. Red correlation bands highlight well marker correlation, inconsistent with the principal sediment transport direction in the considered interval. (single column - colored)

4.1. Sedimentary facies variance minimization

In order to minimize the sedimentary facies variance (e.g., Hale, 2013), the well distality is not taken into account. Figure 10 shows the realization having the lowest cumulative correlation cost computed with Equation (7), i.e., considering that wells have the same distality, and using only lithostratigraphy.

Simulation outcome highlights inconsistent well marker correlations (red correlation bands on Figure 10), for example a well marker interpreted as a patch reef sedimentary facies in the well 1 (between depths $z = 17.7$ m and $z = 18.59$ m) is correlated with a well marker interpreted as an open lagoon in the well 2 (between depths $z = 10.91$ m and $z = 11.03$ m). These inconsistent well marker correlations go against the *principle of correlation* postulated in Section 1.3.

4.2. Sedimentary facies versus well distality

Well correlation computed by minimizing the sedimentary facies variance did not return convincing outcomes. Indeed, lithostratigraphic concepts do not, in general, yield isochronous stratigraphic surfaces. Using Equations (5) and (6) to account distality significantly changes the correlation outcomes as illustrated in Figure 11.

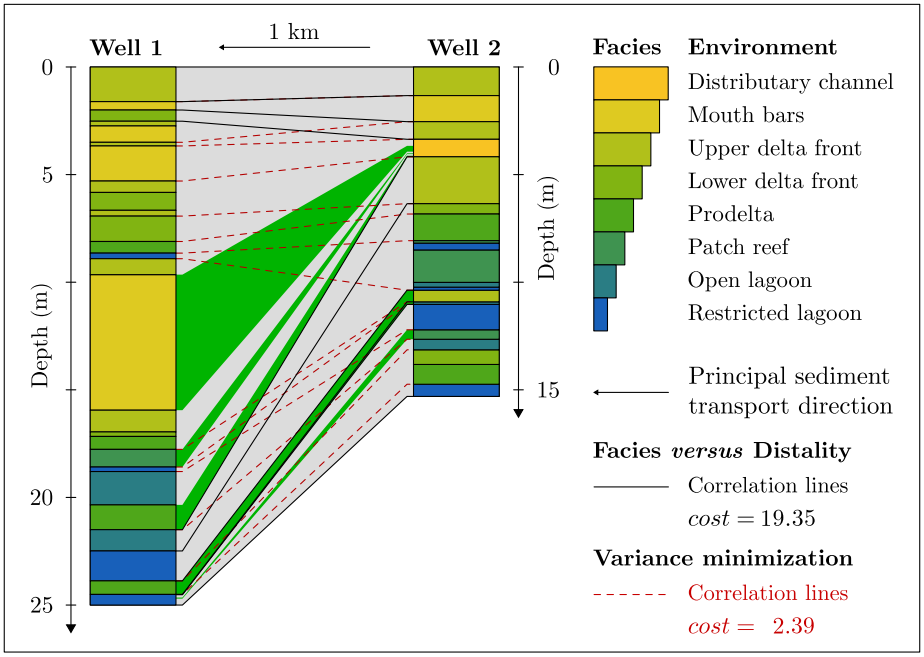

Figure 11: The correlation set having the lowest cumulative correlation cost computed using Equation (8). Green correlation bands highlight well marker correlations which were inconsistent with the sedimentary facies variance minimization and consistent with the proposed rule. Dashed red correlation lines correspond to the most likely correlation set based on the variance minimization (Figure 10). (single column - colored)

The correlation panel illustrated in Figure 11 eases the comparison between the result of the two most likely correlation sets among the n-most likely scenarios computed using lithostratigraphic cost function (7) (dashed red lines) and the distality correlation rule (5) and (6) (full black lines).

Green correlation bands highlight that well markers which were inconsistently correlated using the sedimentary facies variance minimization (red correlation bands in Figure 10) are now consistently correlated using the proposed correlation cost function. This comes from the cost function (5). Moreover, we observe that several facies in one well are correlated with only one facies in the other well. The computer-assisted correlation process generates a gap due to erosion or non-deposition. The depths of these gaps are not fixed *a priori* by the algorithm which only considers a gap cost penalty for each transition, so they emerge from the method in order to maximize the correlation set likelihood. However, if the number of well markers in the different wells differs, multiple correlations to one single marker must occur, and gaps must be simulated.

Another way to visualize a well-to-well correlation problem is to plot a two-dimensional cost matrix representing all well marker associations (Figure 12).

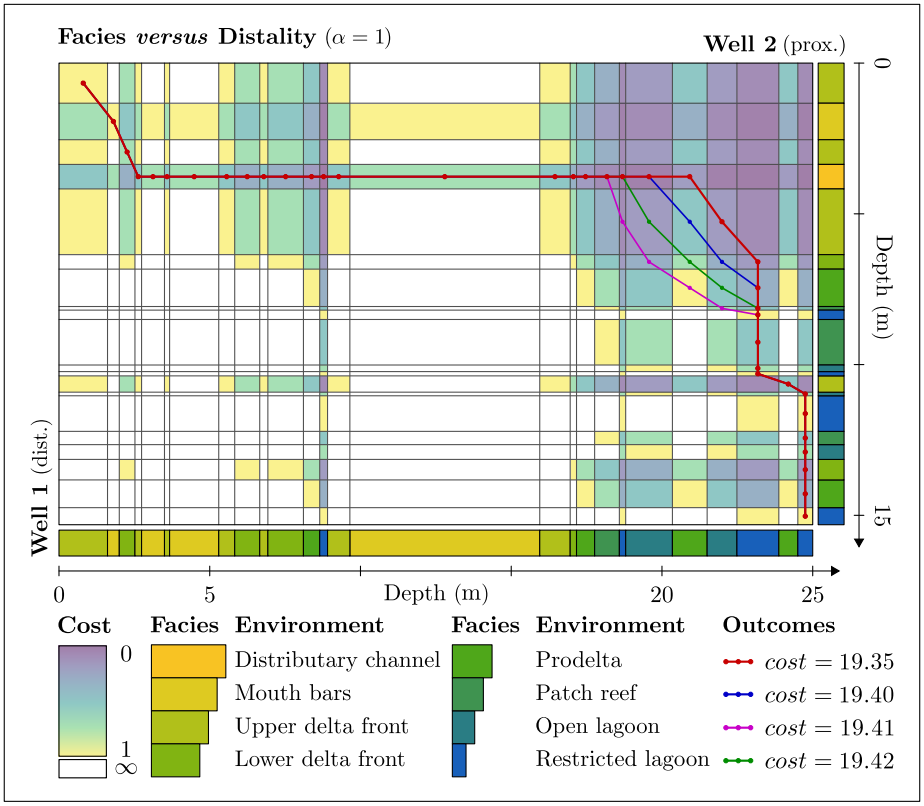

Figure 12: Cost matrix $C[i, j]$ corresponding to the two considered wells. Each cell representing a correlation between two well markers is colored by its correlation cost $c(i, j)$ computed with Equations (5) and (6). The lines correspond to the four most likely scenarios, i.e., the correlation sets with the four lowest cumulative costs computed using Equation (1). Note that the transition costs $t_{i,k}^{j,l}$ associated to the edges or corners of the cost matrix are not visible in this display. (single column - colored)

On this matrix, we can observe that a high number of well marker correlations are excluded thanks to the *principle of correlation* implemented by Equation (5). Indeed, an infinite correlation cost means that the well marker correlation is not consistent. For example, the large mouth bar observed in the well 1 (between depths $z = 9.75$ m and $z = 15.95$ m) can only be associated with mouth bars (between depths $z = 1.33$ m and $z = 2.54$ m) and distributary channels (between depths $z = 3.36$ m and $z = 4.17$ m) in the well 2, which is more proximal. The *principle of correlation* constrains the computer-assisted well-correlation process and generates only admissible scenarios.

In Figure 12, the most likely correlation set is represented by the red line through the cost matrix and each bullet corresponds to each well marker correlation belonging to this correlation set. It is possible to display several scenarios, for

example the four scenarios having the lowest cost in Figure 12. The cost matrix view eases the analysis of differences between correlation sets because we can directly target well marker correlations which are rarely or often simulated.

Moreover, the two-dimensional cost matrix highlights simulated gaps (vertical and horizontal lines) by applying the proposed correlation cost function on the North Sea data set returns two specific types of gaps in this particular scenario (Figure 12):

1. One well marker interpreted as a distributary channel in well 2 (between depths $z = 9.75$ m and $z = 15.95$ m) is correlated with a group of well markers in well 1 (between depths $z = 2.52$ m and $z = 21.50$ m). This significant gap stems from the lack of a proximal facies (distributary channel or mouth bar) below 4.5 m on well 2.

2. Two well markers interpreted as a restricted lagoon in well 2 (between depths $z = 22.49$ m and $z = 23.88$ m and between depths $z = 24.51$ m and $z = 25.00$ m) are correlated with two groups of well markers in well 1 (between depths $z = 6.35$ m and $z = 10.37$ m and between depths $z = 10.91$ m and $z = 15.30$ m).

These observations are consistent with the interpretation of regressive parasequences during which sediments are preferentially deposited along the basin margin rather than in the proximal or distal positions (Galloway, 1989; Homewood et al., 1992; Borgomano et al., 2008; Catuneanu et al., 2010). Hence, this realization, which is defined by the highest likelihood and based on the *principle of correlation*, yields consistent results for the sedimentary facies correlation, that is constrained by the well distality.

However, these results are not consistent with the stratigraphic parasequence interpretation (red triangles in Figure 9). Therefore, this method can help targeting zones of uncertainty in order to make alternative interpretations of core samples and well logs. Alternatively, some method parameters such as the relative well distality (α in Equation (4)) could be tuned to match ancillary constraints, before using the approach to explore uncertainties.

4.3. Impact of the sedimentary facies associations

The correlation cost function is very strict and excludes well marker correlation according to their distality and sedimentary facies interpretation. However, some depositional environments may be laterally equivalent and this equivalence may not be captured by the rules. Moreover, relative well distality may vary through time. This is why we tested it on different sedimentary facies associations (Section 2.3) in order to evaluate the impact of sedimentary facies lateral equivalence. Figure 13 plots one of the most likely computed correlation sets using the facies association A as input against the most likely computed correlation set without facies associations.

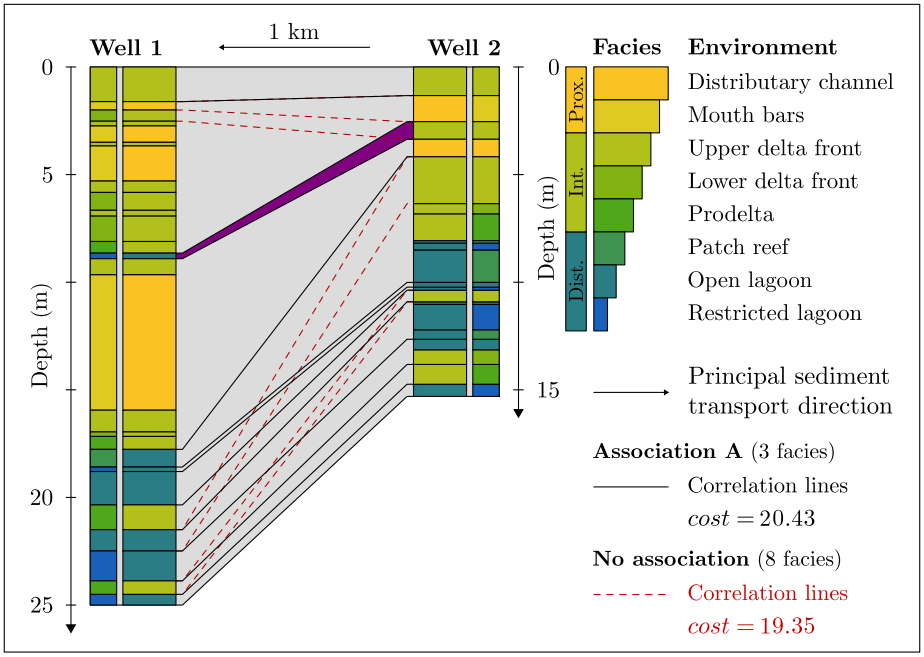

Figure 13: One correlation set having the lowest cumulative correlation cost from the facies association A. The purple correlation band highlights the main difference between this outcome and the outcome obtained without the facies association. Dashed red correlation lines correspond to the most likely correlation set computed without facies association (Figure 11). (single column - colored)

The main difference between this outcome and the most likely correlation set based on the eight sedimentary facies (dashed red correlation lines) is highlighted by the purple correlation band. Without the facies association A, the well marker interpreted as a restricted lagoon in well 1 (between depths $z = 8.65$ m and $z = 8.91$ m) seems to pinch out between the wells (outcome is a gap), but with the facies association A, this well marker is correlated with a well marker interpreted as an upper delta front in well 2 (between depths $z = 2.54$ and $z = 3.36$ m). Correlation sets obtained with the facies associations B and C are illustrated in Figure 14.

The main difference between the outcome computed with 8 facies (Figure 11) and outcomes based on facies associations A, B and C is the number of simulated gaps. Assigning the same value to several facies presenting very close depositional conditions (lateral equivalence) leads to a smaller number of gaps and amounts to a more relaxed interpretation of the *principle of correlation*. Indeed, two facies belonging to the same group have the same code value even if their association goes against the *principle of correlation*.

For example, considering the facies association A, a well marker interpreted as

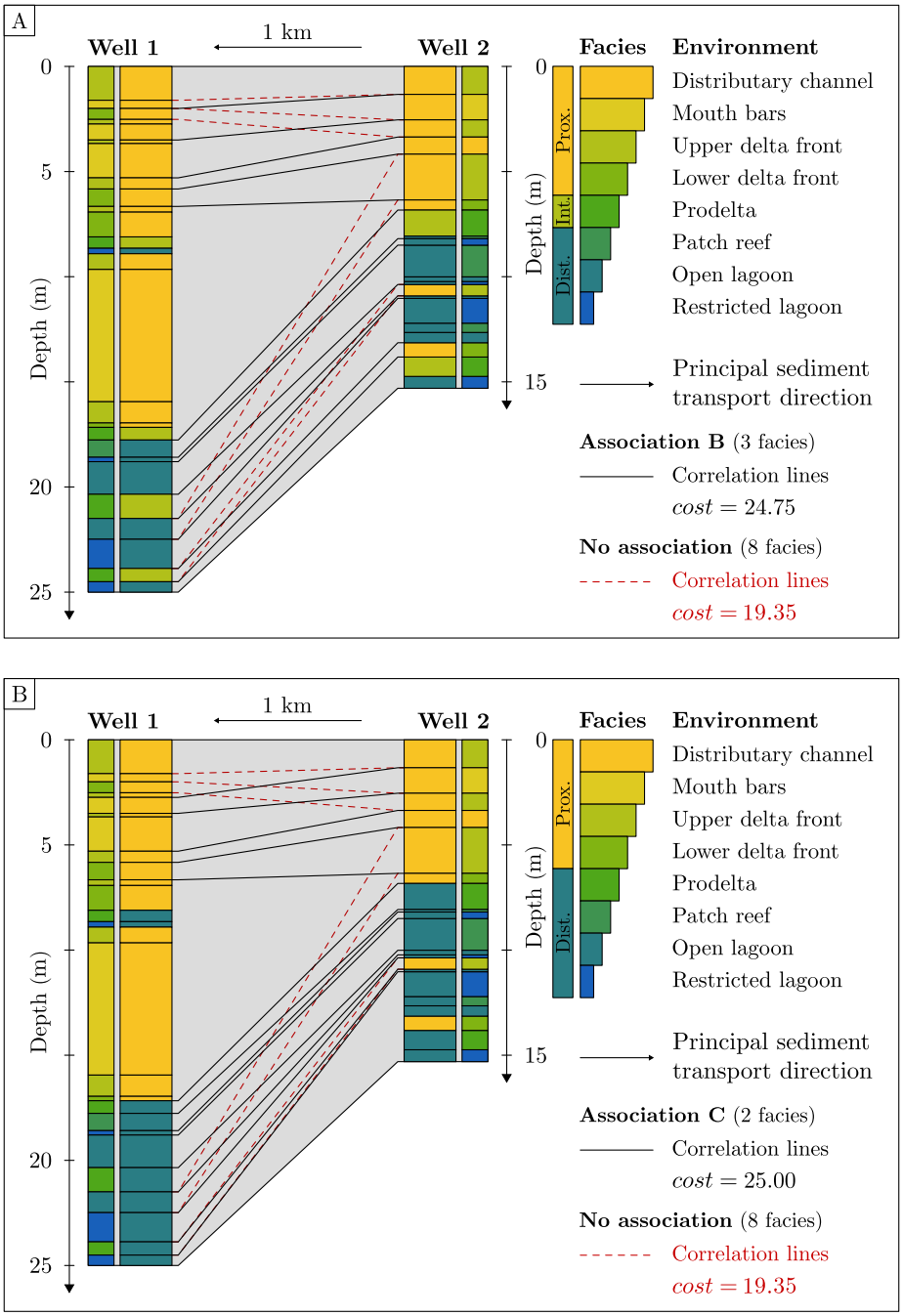

Figure 14: One correlation set having the lowest cumulative correlation cost from the facies association B (A) and from the facies association C (B). Dashed red correlation lines correspond to the most likely correlation set without facies association (Figure 11). (single column - colored)

patch reef (distal facies) in well 1 can be associated to a well marker interpreted as restricted lagoon (distal facies) in the proximal well (Figure 13). The number of plausible well marker correlations (number of painted cells within the cost matrix) should increase directly by associating facies according to their depositional conditions. Increasing the number of plausible correlation may increase the number of diagonal correlation transitions (no gap) and should lead to outcomes with less gaps because of their cost penalty (Section 2.2).

5. Discussion

The proposed method has been applied to two wells of the Gudrun-Sigrun Field area, but it can be extended to n wells as described in Section 2.3. In this case, wells must be classified by their relative positions. Normalization terms defined in Equations (3) and (4) are computed on the entire data set to ensure the consistency of the results. However, the order of well correlation may have a strong impact on the outcomes because only a limited set of scenarios can be propagated through the multi-well correlation process (Edwards et al., 2018).

Independently of the well order, the application of the proposed correlation rule on the Gudrun-Sigrun data set shows that the definition of well distality and sedimentary facies values have a strong impact on the results:

Variation of the principal sediment transport direction. In sedimentary basins, the principal sediment transport direction may vary between two overlapping deltaic lobes, and the presence of several sediment sources may lead to a variation of the principal sediment transport direction in the system. In both cases, the variation of the principal sediment transport direction may be bracketed with reasonable accuracy with dipmeter data. Figure 10 shows the most likely correlation set considering that both wells 1 and 2 have the same distality, i.e., they are located along the strike direction. The associated correlation cost matrix to the correlation given by Equation (7) (i.e., lithostratigraphic correlation) is entirely colored by correlation cost because no well marker correlation is excluded. Figure 11 shows the most likely correlation set considering that wells 1 and 2 are located at the two extremities of the basin along the principal sediment transport direction, and the corresponding correlation cost matrix (Figure 12) illustrates that several well marker correlations are excluded thanks to the *principle of correlation*. Considering two wells, and considering two possible principal sediment transport directions in a circle of 360 degrees, a high number of correlation sets which are plausible in one case may become not possible in the other case. For example, if the relative well position along the distality axis switches, the outcomes might significantly change because of well marker association exclusion changes, thanks the *principle of correlation*.

Variation of the depositional system size with respect to well spacing. Results are also sensitive to the distality variation along a proximal-to-distal transect, which cannot be determined with certainty. To visualize the effects of changing

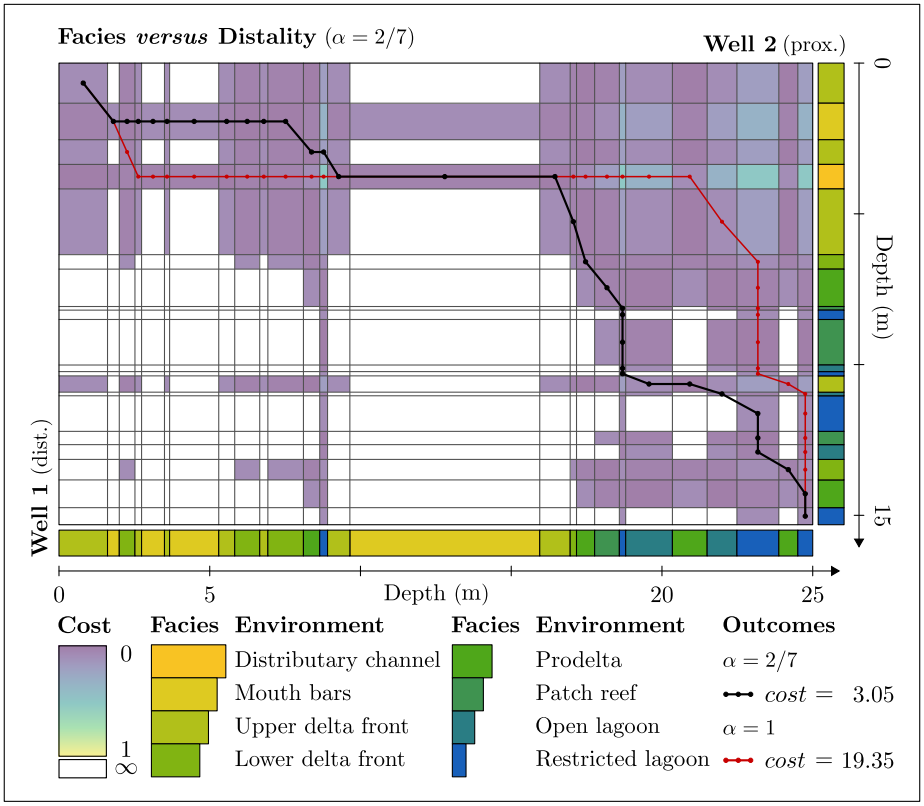

Figure 15: Correlation cost matrix corresponding to chronostratigraphic correlation given by Equation (6) (facies *versus* distality). This case is intermediate between Equations (7) and (8) with $\alpha = 2/7$. The black line corresponds to the most likely correlation set and the red line corresponds to the most likely correlation set computed with $\alpha = 1$ (Figure 12). (single column - colored)

the relative well distality, we computed the cost matrix assuming a depositional system of lateral size equal to 3.5 km, corresponding to a scaling parameter $\alpha = 2/7$ (Figure 15). Comparing the costs of Figures 11 and 15, we see that the distality rule is less discriminant and tends to generate correlation paths closer to the diagonal, i.e., corresponding to a more steady preservation rate in each well in the considered interval.

Both uncertainties about the variation of the principal sediment transport direction and the relative depositional system size can be addressed by playing with the scaling coefficient α in Equation (4):

- A variation of the principal sediment transport direction may be modeled by a scaling coefficient varying between $\alpha = -1$ and $\alpha = 1$. A scaling coefficient $\alpha = -1$ corresponds to the inversion of the principal sediment transport direction and a scaling coefficient $\alpha = 0$ corresponds to the

principal sediment transport direction being perpendicular to the wells.

- A variation of the depositional system size with respect to well spacing may be modeled by a scaling coefficient varying between $\alpha = 0$ and $\alpha = 1$. A scaling coefficient $\alpha = 1$ corresponds to the extreme position of wells within the positional system and a scaling coefficient $\alpha = 0$ corresponds to two wells having the same depositional position within the system.

Modification of sedimentary facies associations. Figures 11, 13 and 14 show chronostratigraphic correlation outcomes computed with Equation (8) using three different facies associations and no facies association. Considering groups of lateral equivalent facies, the correlation cost matrix will be modified because two well markers interpreted as lateral equivalent sedimentary facies are allowed to be correlated. The correlation cost function takes as input parameters the sedimentary facies variation $f(i, j)$ and the well distality variation $d(i, j)$. In the case that two sedimentary facies are laterally equivalent, the variation $f(i, j)$ is null and the correlation cost function will always compute a correlation cost between the two given well markers. Figure 16 shows the correlation cost matrix associated to the facies association A. This highlights that more plausible well marker correlations exist than when considering the initial 8 facies. For instance, well markers interpreted as prodeltas in the proximal well can be correlated to well markers interpreted as upper or lower delta fronts in the distal well (Figure 16).

This computer-assisted method aims to retrieve possible chronostratigraphic lines, and may identify facies association and gaps which are consistent with sedimentary concepts. For example, very thin distal facies or proximal facies may be associated with a thicker succession of intermediate facies during marine regression (Homewood et al., 1992). Considering the consistency of our method applied on sedimentary coastal deltaic data set, it may be used to confront manual parasequence interpretations from well-logs and core-samples, and highlight where uncertainties exist.

However, the correlation set simulation is solely based on correlation cost functions used by the Dynamic Time Warping, so the results are only as good as the input rules (Hale, 2013; Wheeler and Hale, 2014; Lallier et al., 2016; Edwards et al., 2018), and in our case, the likelihood of the *principle of correlation*. For example, the correlation process does not take into consideration the erosion surfaces observed at the top of regressive parasequences. Therefore, additional rules could be integrated in the method. Based on sequence stratigraphy, and considering that during a regressive period sediments are mainly deposited in the intermediate area of the basin, and that during a transgressive period sediments are eroded in the distal part and mainly deposited in the proximal part of the basin as qualitatively illustrated in Figure 2, a transition cost $t_{i-1,i}^{j-1,j}$ may be implemented based on the facies vertical transitions. The thickness of facies intervals could also be considered to further constrain the preservation rate

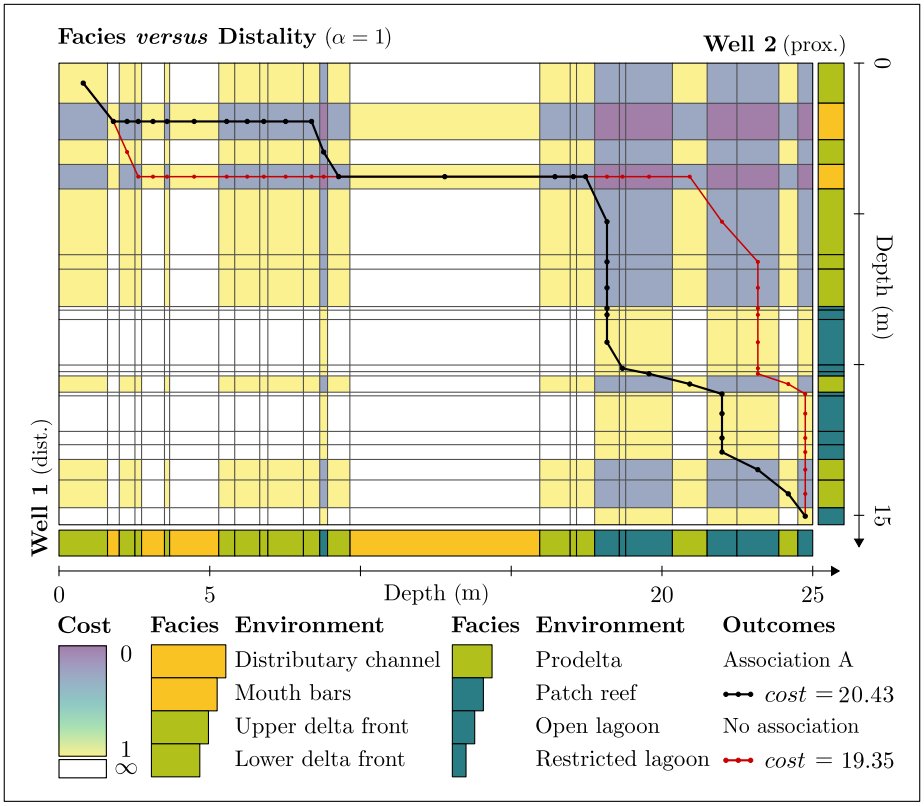

Figure 16: Correlation cost matrix corresponding to chronostratigraphic correlation (Classification A) given by Equation (8) (facies *versus* distality). The black line corresponds to the most likely correlation set (Figure 13) and the red line corresponds to the most likely correlation set computed without facies association (Figure 12). (single column - colored)

emerging from the correlations (Lallier et al., 2013; Hagen et al., 2020).

More generally, the proposed cost normalization, $0 \leq c(i,j) \leq 1$, makes it possible to define multi-criteria correlation costs. Indeed, several independent normalized costs may be combined in the Dynamic Time Warping algorithm by a simple multiplication. As another example, detailed biostratigraphic interpretations are available in the South Viking Graben data set and may be used to constrain the correlation by adding a binary cost function, which allows or excludes a correlation considering the biostratigraphy (Caumon and Antoine, 2019).

Additional data or concepts could also be integrated in the method, preferably as cost function to be combined to the proposed correlation cost function, as an ancillary geological likelihood data to evaluate the results (e.g., de la Varga and Wellmann, 2016). Posterior analysis on the generated stratigraphic model

may be achieved to evaluate the physical likelihood of the correlation outcomes (layer connectivities) like hydraulic or tracer simulation tests (e.g., Baville et al., 2019). Another way to scrutinize and improve the results could be to analyze the geometry of the chronostratigraphic units and their consistency with dipmeter data and subsidence analysis.

Conclusion

In this paper, the purpose of the proposed correlation cost function is to generate several plausible higher-order chronostratigraphic scenarios between lower-order interpreted time lines (e.g., from seismic imaging and biostratigraphic analysis). The obtained correlation results are simulated based on sedimentary facies and well distality interpretations in several wells, and have implications in terms of detailed paleogeography in the considered interval.

The proposed correlation rule is based on the *principle of correlation*: a facies cannot be associated with a depositionally shallower (deeper) facies in a more distal (proximal) well. This method requires sedimentary facies interpretations along well paths and the distality of all wells computed from the well position along a proximal-to-distal transect, to compute a correlation cost for each possible well marker correlation given by Equations (5) and (6).

The overall goal of the method is to generate time lines which reflect both allo cycles and auto cycles. Given the incomplete information available to recover such time lines, ambiguity is clearly expected and it should not be hidden, as it may affect the understanding and the way applied geoscientists model facies, flow units and thin horizontal permeability barriers in subsurface reservoirs (Lallier et al., 2016). The approach proposed in this paper makes it possible to include the concept of distality in such uncertainty quantification and to generate alternative layer connectivities between linear stratigraphic sections.

CRediT author statement

Paul Baville: Conceptualization, Investigation, Methodology, Software, Visualization, Writing (original draft). **Marcus Apel:** Conceptualization, Data Curation, Funding Acquisition, Resources, Validation, Writing (reviewing and editing). **Silvan Hoth:** Conceptualization, Data Curation, Funding Acquisition, Resources, Validation, Writing (reviewing and editing). **Dirk Knaust:** Conceptualization, Data Curation, Resources, Validation, Writing (reviewing and editing). **Christophe Antoine:** Software. **Cédric Carpentier:** Supervision, Writing (reviewing and editing). **Guillaume Caumon:** Conceptualization, Methodology, Supervision, Funding Acquisition, Validation, Writing (reviewing and editing).

Acknowledgments

This work was performed in the frame of the RING project at Université de Lorraine (http://ring.georessources.univ-lorraine.fr). We would like to thank the industrial and academic sponsors of the RING Consortium managed by ASGA and Equinor for their support. The code corresponding to this paper was implemented as a stand-alone C++ and Python algorithm (WeCo) available to RING Sponsors. The authors are grateful to Equinor and the PL025 licence partners Neptune, OMV and Repsol for providing permission to use the Gudrun-Sigrun Field area data set in this work and to publish it.

References

Ainsworth, R.B., Sanlung, M., Duivenvoorden, S.T.C., 1999. Correlation techniques, perforation strategies, and recovery factors: an integrated 3-D reservoir modeling study, Sirikit field, Thailand. AAPG Bulletin 83, 1535–1551. doi:10.1306/E4FD420B-1732-11D7-8645000102C1865D.

Amosu, A., Sun, Y., 2017. WheelerLab: An interactive program for sequence stratigraphic analysis of seismic sections, outcrops and well sections and the generation of chronostratigraphic sections and dynamic chronostratigraphic sections. SoftwareX 6, 19–24. doi:10.1016/j.softx.2016.12.003.

Baville, P., Peisker, J., Caumon, G., 2019. From well logs to stratigraphic layering: Automation, uncertainties and impact on reservoir behavior, in: 81st EAGE Conference and Exhibition, European Association of Geoscientists & Engineers. pp. 1–5. doi:10.3997/2214-4609.201901293.

Bhattacharya, J.P., 2006. Deltas, in: Facies models revisited. SPEM Special Publication. volume 84, pp. 237 – 292.

Bhattacharya, J.P., 2011. Practical problems in the application of the sequence stratigraphic method and key surfaces: Integrating observations from ancient fluvial–deltaic wedges with Quaternary and modelling studies. Sedimentology 58, 120–169. doi:10.1111/j.1365-3091.2010.01205.x.

Borgomano, J.R.F., Fournier, F., Viseur, S., Rijkels, L., 2008. Stratigraphic well correlations for 3-D static modeling of carbonate reservoirs. AAPG Bulletin 92, 789–824. doi:10.1306/02210807078.

Bourquin, S., Rigollet, C., Bourges, P., 1998. High-resolution sequence stratigraphy of an alluvial fan–fan delta environment: Stratigraphic and geodynamic implications – An example from the Keuper Chaunoy Sandstones, Paris Basin. Sedimentary Geology 121, 207–237. doi:10.1016/S0037-0738(98)00081-5.

Catuneanu, O., 2002. Sequence stratigraphy of clastic systems: Concepts, merits, and pitfalls. Journal of African Earth Sciences 35, 1–43. doi:10.1016/S0899-5362(02)00004-0.

Catuneanu, O., Abreu, V., Bhattacharya, J.P., Blum, M.D., Dalrymple, R.W., Eriksson, P.G., Fielding, C.R., Fisher, W.L., Galloway, W.E., Gibling, M.R., Giles, K.A., Holbrook, J.M., Jordan, R., Kendall, C.G.S.C., Macurda, B., Martinsen, O.J., Miall, A.D., Neal, J.E., Nummedal, D., Pomar, L., Posamentier, H.W., Pratt, B.R., Sarg, J.F., Shanley, K.W., Steel, R.J., Strasser, A., Tucker, M.E., Winker, C., 2009. Towards the standardization of sequence stratigraphy. Earth-Science Reviews 92, 1–33. doi:10.1016/j.earscirev.2008.10.003.

Catuneanu, O., Bhattacharya, J.P., Blum, M.D., Dalrymple, R.W., Eriksson, P.G., Fielding, C.R., Fisher, W.L., Galloway, W.E., Gianolla, P., Gibling, M.R., Giles, K.A., Holbrook, J.M., Jordan, R., Posamentier, H.W., Pratt, B.R., Shanley, K.W., Steel, R.J., Strasser, A., Tucker, M.E., 2010. Sequence stratigraphy: Common ground after three decades of development. Fisrt Break 28, 14.

Catuneanu, O., Galloway, W.E., Kendall, C.G.S.C., Miall, A.D., Posamentier, H.W., Strasser, A., Tucker, M.E., 2011. Sequence stratigraphy: Methodology and nomenclature. Newsletters on Stratigraphy , 173–245doi:10.1127/0078-0421/2011/0011.

Caumon, G., Antoine, C., 2019. Stochastic stratigraphic correlation of multiple wells seen as a directed acyclic graph creation problem, in: IAMG 2019, International Association of Mathematical Geosciences, State College, PA, United States.

Driscoll, N.W., Karner, G.D., 1999. Three-dimensional quantitative modeling of clinoform development. Marine Geology 154, 383–398. doi:10.1016/S0025-3227(98)00125-X.

Edwards, J., Lallier, F., Caumon, G., Carpentier, C., 2018. Uncertainty management in stratigraphic well correlation and stratigraphic architectures: A training-based method. Computers & Geosciences 111, 1–17. doi:10.1016/j.cageo.2017.10.008.

Embry, A.E., 2009. Practical sequence stratigraphy. Canadian Society of Petroleum Geologists.

Galloway, W.E., 1989. Genetic stratigraphic sequences in basin analysis I: Architecture and genesis of flooding-surface bounded depositional units. AAPG Bulletin 73, 125–142. doi:10.1306/703C9AF5-1707-11D7-8645000102C1865D.

Hagen, C.J., Reilly, B.T., Stoner, J.S., Creveling, J.R., 2020. Dynamic time warping of palaeomagnetic secular variation data. Geophysical Journal International 221, 706–721. doi:10.1093/gji/ggaa004.

Hale, D., 2013. Dynamic warping of seismic images. GEOPHYSICS 78, S105–S115. doi:10.1190/geo2012-0327.1.

Holbrook, J.M., Bhattacharya, J.P., 2012. Reappraisal of the sequence boundary in time and space: Case and considerations for an SU (subaerial unconformity) that is not a sediment bypass surface, a time barrier, or an unconformity. Earth-Science Reviews 113, 271–302. doi:10.1016/j.earscirev.2012.03.006.

Homewood, P., Guillocheau, F., Eschard, R., Cross, T.A., 1992. Corrélations haute résolution et stratigraphie génétique : une démarche intégrée. Bulletin des centres de recherches exploration - Production Elf-Aquitaine 16, 357–381.

Jerrett, R.M., Bennie, L.I., Flint, S.S., Greb, S.F., 2016. Extrinsic and intrinsic controls on mouth bar and mouth bar complex architecture: Examples from the Pennsylvanian (Upper Carboniferous) of the central Appalachian Basin, Kentucky, USA. GSA Bulletin 128, 1696–1716. doi:10.1130/B31429.1. publisher: GeoScienceWorld.

Johnson, J.G., Murphy, M.A., 1984. Time-rock model for Siluro-Devonian continental shelf, Western United States. GSA Bulletin 95, 1349–1359. doi:10.1130/0016-7606(1984)95<1349:TMFSCS>2.0.CO;2.

Kedzierski, P., Caumon, G., Mallet, J.L., Royer, J.J., Durand-Riard, P., 2008. 3D Marine Sedimentary Reservoir Stochastic Simulation Accounting for High Resolution Sequence Stratigraphy and Sedimentological Rules, in: Eighth Geostatistical Geostatistics Congress, Gecamin, Ltd. p. 657.

Knaust, D., Hoth, S., 2020. Bay-head deltas as hydrocarbon reservoirs: The Middle Jurassic Hugin Formation in block 15/3 of the South Viking Graben, Norway. Marine and Petroleum Geology , 104841doi:10.1016/j.marpetgeo.2020.104841.

Koppka, J., 2015. Revision of the Bivalvia from the Upper Jurassic Reuchenette Formation, Northwest Switzerland: Ostreoidea. OCLC: 1159188872.

Lallier, F., Antoine, C., Charreau, J., Caumon, G., Ruiu, J., 2013. Management of ambiguities in magnetostratigraphic correlation. Earth and Planetary Science Letters 371-372, 26–36. doi:10.1016/j.epsl.2013.04.019.

Lallier, F., Caumon, G., Borgomano, J., Viseur, S., Royer, J.J., Antoine, C., 2016. Uncertainty assessment in the stratigraphic well correlation of a carbonate ramp: Method and application to the Beausset Basin, SE France. Comptes Rendus Geoscience 348, 499–509. doi:10.1016/j.crte.2015.10.002.

Mallet, J.L., 2004. Space–Time Mathematical Framework for Sedimentary Geology. Mathematical Geology 36, 1–32. doi:10.1023/B:MATG.0000016228.75495.7c.

Mitchum, R.M., 1977. Seismic stratigraphy and global changes of sea level: Part 11. Glossary of terms used in seismic stratigraphy: Section 2. Application of seismic reflection configuration to stratigraphic interpretation, in: Seismic

Stratigraphy–Applications to Hydrocarbon Exploration. AAPG Special Volumes. volume 165, pp. 205–212.

Mitchum, R.M., Vail, P.R., Sangree, J.B., 1977. Seismic stratigraphy and global changes of sea level: Part 6. Stratigraphic interpretation of seismic reflection patterns in depositional sequences: Section 2. Application of seismic reflection configuration to stratigraphic interpretation, in: Seismic Stratigraphy–Applications to Hydrocarbon Exploration. volume 165, pp. 117–133.

Nagy, J., Bjørlykke, K., 2015. Stratigraphy, in: Bjørlykke, K. (Ed.), Petroleum Geoscience: From Sedimentary Environments to Rock Physics. Springer, Berlin, Heidelberg, pp. 231–253. doi:10.1007/978-3-642-34132-8_7.

Pels, B., Keizer, J.J., Young, R., 1996. Automated biostratigraphic correlation of palynological records on the basis of shapes of pollen curves and evaluation of next-best solutions. Palaeogeography, Palaeoclimatology, Palaeoecology 124, 17–37. doi:10.1016/0031-0182(96)00017-X.

Qayyum, F., Betzler, C., Catuneanu, O., 2017. The Wheeler diagram, flattening theory, and time. Marine and Petroleum Geology 86, 1417–1430. doi:10.1016/j.marpetgeo.2017.07.034.

Rich, J.L., 1951. Three critical environments of deposition, and criteria for recognition of rocks deposited in each of them. GSA Bulletin 62, 1–20. doi:10.1130/0016-7606(1951)62[1:TCEODA]2.0.CO;2. publisher: GeoScienceWorld.

Ruiz, G., Le Nir, I., 1999. Sequence stratigraphy and facies analysis - Computer aided interpretation and correlation, in: 61st EAGE Conference and Exhibition, European Association of Geoscientists & Engineers. pp. cp–132–00448. doi:10.3997/2214-4609.201408045.

Sakoe, H., Chiba, S., 1978. Dynamic programming algorithm optimization for spoken word recognition. IEEE Transactions on Acoustics, Speech, and Signal Processing 26, 43–49. doi:10.1109/TASSP.1978.1163055.

Sloss, L.L., Krumbein, W.C., Dapples, E.C., 1949. Integrated facies analysis, in: Sedimentary facies in geologic history. Geological Society of America, New York. volume 39, p. 91.

Smith, T.F., Waterman, M.S., 1980. New Stratigraphic Correlation Techniques. The Journal of Geology 88, 451–457. doi:10.1086/628528. publisher: The University of Chicago Press.

Steno, N., 1669. De solido intra solidum naturaliter contento dissertationis prodromus. Florence.

de la Varga, M., Wellmann, J.F., 2016. Structural geologic modeling as an inference problem: A Bayesian perspective. Interpretation 4, SM1–SM16. doi:10.1190/INT-2015-0188.1. publisher: GeoScienceWorld.

Waterman, M.S., Raymond, R., 1987. The match game: New stratigraphic correlation algorithms. Mathematical Geology 19, 109–127. doi:10.1007/BF00898191.

Wheeler, H.E., 1958. Time-Stratigraphy. AAPG Bulletin 42, 1047–1063. doi:10.1306/0BDA5AF2-16BD-11D7-8645000102C1865D. publisher: GeoScienceWorld.

Wheeler, L., Hale, D., 2014. Simultaneous correlation of multiple well logs, in: SEG Technical Program Expanded Abstracts 2014. Society of Exploration Geophysicists, pp. 618–622. doi:10.1190/segam2014-0227.1.

Wu, X., Shi, Y., Fomel, S., Li, F., 2018. Incremental correlation of multiple well logs following geologically optimal neighbors. Interpretation 6, T713–T722. doi:10.1190/INT-2018-0020.1. publisher: GeoScienceWorld.